Structural changes observed during the reversible hydrogenation of $Mg(BH_4)_2$ with Ni-based additives

I. Saldan[1,2], S. Hino[1], T. D. Humphries[1], O. Zavorotynska[1], M. Chong[3], C.M. Jensen[3], S. Deledda[1], B.C. Hauback[1]*

[1]Institute for Energy Technology, Physics Department, P.O. Box 40, NO-2027 Kjeller, Norway, Tel:+47 6380-6078 Fax:+47 6381-0920, e-mail: bjorn.hauback@ife.no

[2]Ivan Franko National University of L'viv, Department of Physical and Colloid Chemistry, 6 Kyryla and Mefodia Str., UA-79005 L'viv, Ukraine

[3]University of Hawaii, Department of Chemistry, Honolulu, HI 96822, USA

The decomposition and rehydrogenation of γ-$Mg(BH_4)_2$ ball milled together with 2 mol% of Ni-based additives, Ni_{nano}; $NiCl_2$; NiF_2; Ni_3B, has been investigated during one hydrogen desorption-absorption cycle. Under the applied ball-milling conditions, no mechanochemical reactions between γ-$Mg(BH_4)_2$ and Ni_{add} were observed. Hydrogen desorption carried out at temperatures 220-264 ºC resulted for all samples, in partial decomposition of $Mg(BH_4)_2$ and formation of amorphous phases, as seen by Powder X-ray Diffraction (PXD). PXD analysis after rehydrogenation at temperatures 210-262 ºC and at pressures between 100 and 155 bar revealed increased fractions of crystalline β-$Mg(BH_4)_2$, indicating a partial reversibility of the composite powders. The highest amount of $[BH_4]^-$ is formed in the composite containing Ni_3B. Analysis by X-ray Absorption Spectroscopy (XAS) performed after ball milling, after desorption and after absorption shows that the Ni_3B additive remains unaffected, whereas $NiCl_2$ and NiF_2 additives react with $Mg(BH_4)_2$ during the hydrogen desorption-absorption,

and forming compounds with a local structure very similar to that of amorphous Ni_3B. Multinuclear NMR spectroscopy confirms the partial reversibility of the system, as well as the formation of $[B_{10}H_{10}]^{2-}$ during hydrogen absorption. The presence of $[B_nH_n]^{2-}$ (n = 10; 12) was also detected by infrared (IR) spectroscopy of the dehydrogenated and rehydrogenated samples. The IR measurements give no clear indication that ions containing B–H–B bridged hydrogen groups were formed during the H-sorption cycle.

Keywords: Magnesium borohydrides, Nickel boride; Polyboranes; PXD; XAS, NMR, IR.

*Corresponding author

1. Introduction

Magnesium borohydride, $Mg(BH_4)_2$, is one of the most promising hydrogen storage materials due to its theoretical hydrogen capacity of 14.9 wt%.[1] However, its application is hindered by poor kinetics and lack of reversibility. The decomposition of $Mg(BH_4)_2$ occurs via several steps and the resulting products and intermediates vary depending on the experimental conditions.[2-6] The main hydrogen release in pure $Mg(BH_4)_2$ occurs between 270 and 320 ºC. In this temperature region, a variety of intermediate amorphous magnesium polyboranes are formed before decomposition to MgH_2 and amorphous boron. The formation of stable higher polyborane intermediates, such as $MgB_{12}H_{12}$,[7,8] has been proposed to be the main factor hindering reversible hydrogenation of $Mg(BH_4)_2$. The icosahedral framework in $MgB_{12}H_{12}$ and that of bulk boron is a reason for the thermal stability of the polyboranes.[9] On the other hand, the synthesis of $Mg(BH_4)_2$ from lower polyboranes (e.g. $Mg(B_3H_8)_2$) has been demonstrated at a relatively low hydrogen pressure and temperature (~120 bar of H_2 and 250 ºC).[10] Decomposition of $Mg(BH_4)_2$ to $Mg(B_3H_8)_2$ is reported to be reversible with theoretical hydrogen storage capacity of 2.5 wt%.[10]

An additive that changes the reaction pathway and thus inhibits the formation of stable higher polyboranes, is one of the possibilities that could improve the reversibility of H-sorption in $Mg(BH_4)_2$. Development of effective additives to improve the hydrogen desorption-absorption is therefore crucial to be solved before use as a hydrogen storage material.

Transition metals have the ability to bond hydrogen in a variety of stoichiometries. This promotes fast dissociation of molecular hydrogen into atomic hydrogen or its recombination back to hydrogen molecules.[11] Nickel additives have recently gained interest for their catalytic activity towards the reversible hydrogenation of complex hydrides. The

valence of Ni in the $NiCl_2$-activated $LiBH_4$+0.5MgH_2 and $Li_3BN_2H_8$ hydrogen storage materials is close to zero and invariant during hydrogen cycling when analyzed by X-ray Absorption Spectroscopy (XAS).[12,13] Moreover, Ni-doped $LiBH_4$+0.5MgH_2 initially forms amorphous Ni_3B, which is partially converted to amorphous Mg_2NiH_x upon hydrogen absorption. Surface calculations performed using density functional theory suggest that the lowest kinetic barrier for H_2 chemisorption occurs on the Ni_3B (100) surface.[12] The order of catalytic activity of Ni additives towards the hydrogenation of benzene was established to be as follows: nanocrystalline Ni > nanoamorphous Ni–B alloy > crystalline Ni ≈ crystalline Ni_3B.[14] Ni additives, Ni nanoparticles, Ni_3B, $NiCl_2$, NiF_2 and Ni (65 wt % on Si/Al_2O_3), have also been demonstrated to decrease the temperature of hydrogen desorption in $NaBH_4$ by at least 60 ºC.[15]

In the present work, four different Ni-based additives, Ni_{nano}; $NiCl_2$; NiF_2; Ni_3B, have been investigated as possible catalysts towards reversible $Mg(BH_4)_2$ decomposition. Qualitative analysis of the additives during hydrogen desorption-absorption was performed by X-ray Absorption Near Edge Spectroscopy/Extended X-ray Absorption Fine Structure (XANES/EXAFS) as a “finger print” method and their Fourier Transforms to determine the interatomic distances between Ni and other neighboring atoms. The borane species present after desorption-absorption were characterized by ^{11}B and ^{1}H NMR and infrared (IR) spectroscopy.

2. Experimental methods

Commercial γ-$Mg(BH_4)_2$ (≥95%, Sigma Aldrich) was used to prepare $Mg(BH_4)_2$–Ni_{add} (Ni_{add} = Ni_{nano} (30 nm, nanostructured & Amorphous Inc); $NiCl_2$ (99.99 %, Sigma Aldrich); NiF_2 (Sigma Aldrich) and Ni_3B (synthesized in-house)) composites with 2 mol% of

additives by ball-milling. Synthesis of Ni_3B was carried out as described by Kapfenberger et al.[16] An aqueous 2 M solution of $NaBH_4$ was added drop-wise to an ice-cooled 0.27 M aqueous solution of $NiCl_2$ over 45 min, during which effervescence and formation of a black precipitate was observed. The precipitate was then collected by filtration and washed with water, followed by EtOH. The amorphous solid was allowed to dry in air overnight, giving a yield of 62 %. The identity of the amorphous powder was confirmed by Powder X-ray Diffraction (PXD) after annealing a small quantity at 350 ºC for 1.3 h. PXD analysis indicated the presence of Ni_3B as the major phase (ICDD PDF 00-001-1260) with some metallic Ni. The amorphous powder was used as the additive.

Milling was conducted in a Fritsch Pulverisette 7 planetary mill with tempered steel vials (26 ml volume) and balls (10 mm diameter) in Ar atmosphere. A ball-to-powder mass ratio of 40:1 was employed, with a milling time of 1 h at a speed of 300 rpm. All powder manipulations were carried out in MBraun Unilab glove boxes filled with purified argon (<1 ppm O_2/H_2O).

Hydrogen sorption measurements were carried out in an in-house manufactured Sievert's type apparatus.[17] All $Mg(BH_4)_2$–Ni_{add} composites were dehydrogenated under static vacuum (~10^{-5} mbar) and rehydrogenated under 100-155 bar of H_2. The hydrogenation reaction conditions of all composites are summarized in Table 1.

PXD patterns were collected in Debye-Scherrer geometry using CuKα radiation (λ = 1.5418 Å), using a Bruker AXS D8 Advance Diffractometer equipped with a Göbbel mirror and a LynxEye 1D strip detector. The diffraction patterns were obtained using rotating boron glass capillaries, filled and sealed under Ar atmosphere. Small amounts of pure Si (ABCR, APS 1−5 μm, 99.999%) were added as an internal standard. Data acquisition was restricted to 2θ = 5−60º, with $\Delta 2\theta$ = 0.02º and 2 s/step scanning rates.

EXAFS spectra were collected at beamline I811 at MaxLab (Lund, Sweden) in the energy range 8200-9000 eV of Ni K-edge (8331.4 eV) at room temperature.[16] Boron nitride (BN)-2mol% Ni_{nano}, $NiCl_2$, NiF_2, and Ni_3B mixtures were measured for reference. Finely ground powders were pressed into pellets, which were mounted into special aluminum plates. To avoid oxidation, the plates were covered by polyimide film adhered by high vacuum grease. EXAFS data were measured in fluorescence mode, six times for each sample (where four quick scans were used for sample adjustments). Two step scans were measured in pre edge and edge regions with counting time 0.5 s and in EXAFS region – 20 s per point. All presented data analyses were performed using ATHENA and ARTEMIS software.[19]

^{1}H and ^{11}B NMR solution spectroscopy was carried out on a Varian Unity Innova 500 MHz spectrometer with ^{11}B chemical shifts referenced to $BF_3 \cdot OEt_2$ ($\delta = 0$ ppm) at 20 ºC. All ^{1}H were referenced to the D_2O peak at 4.79 ppm. Deuterium oxide was chosen as the solvent for the NMR studies because it allowed for the most complete dissolution of the sample powders.[10] As a consequence, however, any boranes possessing open cage structures, such as *nido* or *arachno*boranes tend to hydrolyze usually appearing somewhat downfield of 0 ppm.[20-22]

Attenuated Total Reflection Fourier Transformed Infrared (ATR FT-IR) spectra were measured on a Bruker Alpha-Platinum infrared spectrometer upon a diamond crystal. The spectra were obtained in the range of 4000-400 cm^{-1}, with a resolution of 2 cm^{-1}, with 32 scans averaged for each spectrum and the background. The samples were measured without any dilution. All of the IR measurements were conducted in an argon-filled glove box.

3. Results and discussion

3.1 Hydrogen desorption-absorption and PXD analysis

Each of the milled $Mg(BH_4)_2$–Ni_{add} composites were dehydrogenated in the Sieverts type apparatus at temperatures between 220 and 264 ºC. This temperature range was chosen to promote partial decomposition and, in particular, the formation of $Mg(B_3H_8)_2$ rather than the thermodynamically stable polyboranes, e.g. $MgB_{10}H_{10}$ or $MgB_{12}H_{12}$. These conditions are close to those utilized in a previous study in which $Mg(B_3H_8)_2$ was demonstrated to be reversibly hydrogenated to $Mg(BH_4)_2$.[10] Hydrogen absorption was then performed on the dehydrogenated powders in order to reform $Mg(BH_4)_2$. The experimental conditions along with quantitative results for desorption-absorption are given in Table 1.

The results of the desorption experiments on the composites containing Ni_{nano}, $NiCl_2$ and Ni_3B indicate that the hydrogen content (approximately ~2.5 wt% of H_2) corresponds to what is theoretically expected for the formation of $Mg(B_3H_8)_2$. However, the time of 60 h required for hydrogen desorption is significantly reduced compared to 5 weeks at 200 ºC reported for pure $Mg(BH_4)_2$.[10] This suggests an apparent effectiveness of Ni-based additives in promoting hydrogen desorption in $Mg(BH_4)_2$, although the higher operating temperatures used in our work during desorption also play a beneficial role for improving the desorption kinetics. The high desorption value obtained for $Mg(BH_4)_2$–NiF_2 (~6.5 wt% of H_2) might be due to the effect of a slightly higher temperature. After desorption each sample absorbed 1–2 wt% H_2. The reasons for this discrepancy can be ascribed to several interplaying factors: 1) the gas desorbed was not pure hydrogen but consisted also of, for instance, B_2H_6; 2) some irreversible phases were formed during desorption; and 3) the absorption pressure was not high enough to completely reform $Mg(BH_4)_2$.

PXD patterns of the $Mg(BH_4)_2$–Ni_{add} composites, in the as-milled, desorbed and absorbed state, were collected for phase identification. Si powder was used as an internal standard to enable Bragg peak position correction. Although moderate milling conditions were employed, slight amorphization of γ-$Mg(BH_4)_2$ takes place during milling (see PXD for as-milled samples: patterns (i) in Fig. 1), as previously reported by Li et al.[23] This may be because the ball milling can easily induce the collapse of the highly porous structure of γ-$Mg(BH_4)_2$.[24] The remaining fraction of crystalline γ-$Mg(BH_4)_2$ undergoes an irreversible phase transformation via the ε polymorph to β-$Mg(BH_4)_2$ upon heating to 200 ºC.[25] This is in agreement with our PXD results: in all samples desorption is not complete and the remaining fraction of $Mg(BH_4)_2$ is theβ-modification (see PXD after desorption: patterns (ii) in Fig. 1). After absorption of H_2, all $Mg(BH_4)_2$–Ni_{add} composites exhibit an increased relative intensity of the β-$Mg(BH_4)_2$ peaks, when compared with the PXD patterns after desorption. This indicates that during rehydrogenation, magnesium borohydride partially reforms from the desorbed samples.

While PXD analysis confirms slight amorphization of γ-$Mg(BH_4)_2$ in all as-milled $Mg(BH_4)_2$–Ni_{add} composites, it does not provide much information about the nature of the Ni additives. $NiCl_2$ and Ni_{nano} can still be detected after milling, however, the Bragg peaks for NiF_2 are obscured by those for $Mg(BH_4)_2$ therefore rendering the identification of the additive problematic. Furthermore, since amorphous nickel boride was used for the composite preparation, this additive is not detectible by PXD. All Ni additives (with exception for Ni_{nano}) were not detected by PXD after the hydrogen desorption-absorption cycle. Therefore X-ray Absorption Spectroscopy (XAS) was used as a suitable technique for monitoring the local chemical structure of the Ni additives.

3.2. X-ray absorption spectroscopy at the Ni K-edge

XAS at the Ni K-edge, measured in the range of 8200–9000 eV, was used to determine the local structure around the Ni atoms. EXAFS represents the fractional change in the absorption coefficient induced by neighboring atoms and contains only structural information. Fig. 2 illustrates the normalized absorption spectra of the $Mg(BH_4)_2$–Ni_{add} composites (as-milled and after hydrogen desorption-absorption).

The individual spectral profiles of the as-milled samples in Fig. 2*a* are noticeably different, indicating that each additive has dissimilar neighboring atoms around the respective Ni atoms. Each profile is basically identical to that of each reference materials (shown in supporting information), suggesting that the structure of the various Ni-additives were preserved after milling. However, after hydrogen desorption-absorption, Fig. 2(*b*), the EXAFS spectra are nearly undistinguishable from one another. The two insets in Fig. 2 show the XANES data in the energy region of 8200–8390 eV. The $Mg(BH_4)_2$ composites containing $NiCl_2$ and NiF_2 show a small shift of the Ni-edge to higher energies compared to Ni_{nano} and Ni_3B indicating that the Ni exists in a higher oxidation state (inset in Fig. 2*a*). When the metal center possesses a higher oxidation state, the attraction between the electrons and nucleus increases as the removal of the valence electrons reduces the shielding of the core electrons from the nucleus. For the rehydrogenated $Mg(BH_4)_2$–Ni_{add} composites, all of the XANES spectra (inset in Fig. 2(*b*)) are almost identical, indicating that the Ni atoms exist in the same oxidation state. In light of these facts, it is proposed that during hydrogen desorption-absorption, the Ni additives react to form a new Ni compound that might be responsible for the enhanced desorption activity of $Mg(BH_4)_2$.

Fourier Transform (FT) of the XAFS data is useful for separating XAFS frequency functions and converting them to corresponding peaks in real space, with the aim to extract the interatomic distances (*R*) between the absorber and backscattering coordination shell. FT

of the k^3-weighted $\chi(k)$ function for the milled, dehydrogenated and rehydrogenated $Mg(BH_4)_2$–Ni_{add} composites is shown in Fig. 3. For each milled composite, the atomic distribution around the Ni atom is identical to that of the respective Ni containing reference samples. This suggests that the milling process does not result in chemical reaction between the $Mg(BH_4)_2$ and the additives.

Analysis of the Ni nanopowder composite samples indicates that the main peak at 2.2 Å is from the Ni nearest neighbor and peaks in the range of 3 – 5 Å correspond to 2nd; 3rd and 4th nearest shells. The Ni–Ni distances measured in the milled and desorbed $Mg(BH_4)_2$–Ni_{nano} composites are very similar to the Ni nanopowder reference sample in Fig. 3(*a*). This suggests an almost identical Ni local structure and confirms the presence of metallic Ni as identified by PXD. However, the intensities of peaks above 3 Å are reduced compared to the 1st peak in the desorbed sample, indicating a lower degree of long-range order. After hydrogen absorption, the intensity of the main peak at ~2.1 Å has decreased and peaks above 3.5 Å are barely visible. This is indicative of a higher degree of disorder in the medium- and long range around the central Ni atom.

The spectra of the $Mg(BH_4)_2$–$NiCl_2$ and $Mg(BH_4)_2$–NiF_2 composites (Figs. 3*b*-*c*) show an alternative trend. For these Ni additives, the first coordination shell around the central Ni atom consists of lighter atoms (Cl or F). After hydrogen desorption the XANES and EXAFS profiles of these samples are dramatically altered from their initial state, suggesting the local environment of the Ni atom is chemically and structurally different. At the same time it is similar to that observed for Ni_{nano}. Following hydrogen absorption, these configurations remain, suggesting that the central Ni atom undergoes no further reaction during the hydrogenation process.

The FT for the $Mg(BH_4)_2$–Ni_3B composites after milling, desorption and absorption (Fig. 3*d*) show similar patterns. The shoulder at 1.6 Å corresponds to the nearest B shell and the main peak at ~2.1 Å corresponds to the nearest Ni shell.[26] Absence of major peaks above 3 Å implies medium- and long range disorder in the local environment of Ni. This is due to the amorphous nature of the as-prepared Ni_3B. The lack of difference in the long range order suggests that the crystallization of amorphous NiB_3, which is possible at the temperatures used for absorption, has not occurred.[26-30] This is confirmed by PXD analysis (see Fig. 1*d*).

It should be noted that for all rehydrogenated $Mg(BH_4)_2$–Ni_{add} composites, XANES and EXAFS profiles are almost identical (Fig. 2*b*) and are similar to those of amorphous Ni_3B (Fig. 3*d*). This suggests that in all composites, a Ni species with a local structure similar to that of Ni_3B forms after hydrogen desorption-absorption. The FT for all rehydrogenated $Mg(BH_4)_2$–Ni_{add} composites together with two references of Ni_3B are shown in Fig. 4. In fact, after hydrogen desorption-absorption the local structure of Ni_{add} is very similar to that of the synthesized amorphous Ni_3B (ref in Fig. 4). In addition to that, only FT of crystalline Ni_3B (calculated from theoretical FEFF files using crystallographic data) shows peaks at ~3.1; 3.6 and 4.3 Å. These quite intense peaks insist on long range ordering around Ni that is not observed for amorphous Ni_3B or rehydrogenated $Mg(BH_4)_2$–Ni_{add} composites. The obtained XAS results ~~conclusions~~ are not surprising, as a recent cycling study of $NaBH_4$ with similar Ni additives yielded identical observations by PXD.[15] It is reasonable that during the decomposition of $Mg(BH_4)_2$ composites, chemical reaction between the Ni additives and the intermediate B-containing species prevails to form a thermodynamically stable Ni_xB_y species. In this work, Ni_3B appears to be the most stable Ni_xB_y species as no further reaction occurs during subsequent hydrogenation.

Formatted: Font: Italic

Formatted: Font: Italic

Formatted: Subscript

Formatted: Subscript

3.3. ^{1}H and ^{11}B NMR spectroscopy studies

In an effort to understand the phases that are formed during desorption and absorption, ^{1}H and ^{11}B NMR spectroscopy studies were performed in D_2O on each of the $Mg(BH_4)_2$–Ni_{add} composites after H-sorption and on pure γ-$Mg(BH_4)_2$ as reference. NMR spectroscopy enables the identification of phases that, if amorphous, cannot be detected by PXD. This is particularly helpful for the study of borane containing species. The ^{1}H NMR spectra of $Mg(BH_4)_2$–Ni_{add} composites after desorption and absorption are presented in Fig. 5. A broad multiplet consisting of at least a quadruplet is observed in all spectra between 0.25 and −0.45 ppm after desorption, indicative of $Mg(BH_4)_2$. This suggests that total decomposition of γ-$Mg(BH_4)_2$ did not occur during hydrogen desorption, which was also evident by PXD (Fig. 1). Other broad features are observed but their intensities are too weak to unambiguously assign them.

The decoupled ^{11}B NMR spectra illustrated in Fig. 6 provide a clear insight into the boron phases produced during hydrogen desorption-absorption of the $Mg(BH_4)_2$–Ni_{add} composites. The resonance at –42 ppm in all spectra is attributed to $Mg(BH_4)_2$ and confirms the incomplete decomposition of the initial $Mg(BH_4)_2$–Ni_{add} composites.[31,32] All desorbed composite samples feature a resonance at –31 ppm, which is the most intense in ^{11}B NMR spectra apart from the $Mg(BH_4)_2$–Ni_3B sample. After hydrogenation, this peak disappears completely, while the resonances at –42 ppm ($[BH_4]^-$) and –30 ppm, which are also observed after desorption, grow in intensity.

The peak at –31 ppm can obviously be assigned to a reversible phase, which from general consensus can be attributed to $[B_3H_8]^-$.[10,32] The resonance at –30 ppm can be assigned to $[B_{10}H_{10}]^{2-}$. Additional weak peaks are observed between –12 and –24 ppm, where the resonances for the $[B_2H_6]^{2-}$, $[B_5H_8]^-$, and $[B_{12}H_{12}]^{2-}$ anions are expected. This implies that the formation of the decomposition products $[B_2H_6]^{2-}$, $[B_5H_8]^-$, and $[B_{12}H_{12}]^{2-}$ is limited but not completely avoided even at a temperature below 264 ºC. Their concentration does not

increase after hydrogenation, confirming their thermodynamic stability and their role in inhibiting reversibility of $Mg(BH_4)_2$. The fraction of $[B_{10}H_{10}]^-$ is significant already after desorption and increases after hydrogenation (Table 2). This might suggest that the Ni additives, which were expected to enhance the reversible hydrogenation of $Mg(BH_4)_2$, are also promoting the formation of $[B_{10}H_{10}]^{2-}$.

Another major resonance observed in the decoupled ^{11}B NMR spectra is a broad feature at 4 ppm attributed to hydrolyzed borane derivatives, which are likely reaction products of boranes possessing open cage structures, such as *nido* or *arachno* boranes, and D_2O solvent.[20-22] Although the measurements are conducted promptly after addition of the D_2O solvent, this reaction is unavoidably rapid but the use of this solvent has been identified as the most efficient at dissolving the majority of the products associated with the reversible hydrogenation of $Mg(BH_4)_2$. On the other hand, IR analysis (see section 3.4 below) shows that the sample was possibly already contaminated with borates following the ball milling. Thus the peak at 4 ppm can be at least partially due to these impurities. The amorphous and insoluble Ni_3B additives formed during desorption are not observed by liquid state NMR spectroscopy.

The relative concentration of the boron containing species measured by ^{11}B NMR spectroscopy is summarized in Table 2. The data in the table suggest that the Ni additives promote both $[BH_4]^-$ and $[B_{10}H_{10}]^{2-}$ formation from $[B_3H_8]^-$ during hydrogenation. The least relative concentration of the undesirable $[B_{10}H_{10}]^{2-}$ is formed upon absorption in presence of Ni_3B. There is an increase in relative concentration of $[BH_4]^-$ in the Ni_{nano} containing sample from 0.25 to 0.94 and an increase from 0.18 to 0.34 in the NiF_2 containing sample, but the most dramatic increase in integrated relative concentration is that of $[B_{10}H_{10}]^{2-}$.

3.4. Infrared study

The IR spectra of the ball milled, dehydrogenated and rehydrogenated samples of $Mg(BH_4)_2$–Ni_{add} composites and pure **γ**-$Mg(BH_4)_2$ are shown in Fig. 7. For **γ**-$Mg(BH_4)_2$ (Fig. 7*a*) the IR data exhibits the internal vibrations of $[BH_4]^-$ ions in the 2900-600 cm^{-1} region. The B–H fundamental stretching modes are centred at 2270 cm^{-1}, and the bending modes are located at *ca.* 1420 (broad), 1260 and 1130 cm^{-1}.[33] The peaks at 2660 and 2400 cm^{-1} are assigned to the overtones and combinations of $[BH_4]^-$ stretching and bending. According to Raman measurements and DFT calculations, $Mg(BH_4)_2$ does not have normal modes of vibrations in the 670-1120 cm^{-1} region.[33] Therefore the peaks at 913 and 706 cm^{-1} may be attributed to impurities, for example, boron oxides due to small air contamination during sample preparation.

The spectrum of $Mg(BH_4)_2$ is slightly altered after milling with the Ni containing additives. The principle stretching and bending modes of $[BH_4]^-$ are preserved, although their position is slightly shifted by 2-5cm^{-1}. For the as-milled $Mg(BH_4)_2$–NiF_2 composite (Fig. 7c) an additional peak at 1194 cm^{-1} is clearly distinguishable. These changes may be induced by slight disorder in the $[BH_4]^-$ structure and local environment.

The spectra of the samples after desorption exhibit an overall decrease in the intensities of the B–H stretching and bending bands, which is indicative of a decreased amount of $[BH_4]^-$ groups compared to the spectra of ball-milled compounds. The fingerprint spectrum of $Mg(BH_4)_2$, however, is still recognizable in all spectra after desorption. This is consistent with the PXD and NMR results, which identifies a small amount of $[BH_4]^-$ in all the samples after desorption. Additionally, for the NiF_2-milled sample, a weak absorption peak with a distinct maximum at *ca.* 2540 cm^{-1} appears. This is the region (between 2550 and 2400 cm^{-1}) where the B–H stretching of the *closo* boranes $[B_{12}H_{12}]^{2-}$ and $[B_{10}H_{10}]^{2-}$ is expected as strong bands centred at 2485 and 2467 cm^{-1}, respectively.[34] $[B_{12}H_{12}]^{2-}$ has additional IR-active vibrations at 1070 cm^{-1} (H–B–B bending, medium in intensity), and at

720 cm^{-1} (B–B stretching, medium); $[B_{10}H_{10}]^{2-}$ also absorbs at 1030 cm^{-1} (H–B–B bending, medium in intensity), and 720 cm^{-1} (B–B stretching, medium).[34] The latter peak is considered to be a fingerprint of *closo* boranes.[34] Based on the very weak intensity of the B–H stretching peaks, it is possible that the B–B–H bending and B–B stretching is obscured in the 1100700 cm^{-1} region. New small peaks at 770 and 747 cm^{-1}, where B–B–H bending is expected, appear in the spectra of all samples after desorption but their origin is unclear.

In the spectra of Ni_{nano}- and NiF_2-containg samples after absorption (Fig. 7*a*-*b*), the intensity of the bands due to $[BH_4]^-$ and $[B_nH_n]^{2-}$ increases. The intensity of the vibrations due to $[BH_4]^-$ remains almost unchanged after hydrogen absorption in the $NiCl_2$ and Ni_3B composites. These findings are consistent with the changes in the relative concentrations of these moieties identified by NMR. Finally, it can be noted that the strongest peaks due to $[B_nH_n]^{2-}$ bending are present in the NiF_2-containing composite, and the weakest in the one with Ni_3B. These samples were treated at the highest and the lowest temperature, respectively. On the other hand, it is important to point out that the relative intensities of the IR vibrations of $[BH_4]^-$ and $[B_nH_n]^{2-}$ do not necessarily reflect the relative concentration of these species in the mixture. The intensities of the IR peaks in attenuated total reflection measurements, used in this work, strongly depend on the refractive indexes of the materials. Comparing the intensities ratios of different samples, however, is reasonable.

The ^{11}B-NMR results indicate $[B_3H_8]^-$ as the main phase of the dehydrogenated samples and the significant decrease in its amount upon re-absorption. However, the IR data do not unambiguously confirm the presence of the $[B_3H_8]^-$ in the dehydrogenated samples. An important distinguishable IR feature of these types of compounds is the B–H stretching of the B–H–B *bridged* hydrogen found as low as 2150-2000 cm^{-1}. This region is almost unaffected in the samples upon cycling (Fig. 7, desorption and absorption).

4. Conclusions

γ-$Mg(BH_4)_2$ was milled with a variety of Ni-based additives, Ni_{nano}, $NiCl_2$, NiF_2 and Ni_3B, to study their effect on the reversible hydrogenation of the borohydride. Powders were sampled after milling, hydrogen desorption-absorption to monitor the structural changes in the hydrogen-containing phases with PXD, XAS, NMR and IR spectroscopies. The key conclusions are:

1) Chemical reactions between the Ni-based additives and γ-$Mg(BH_4)_2$ do not take place during ball milling, although the crystallinity of the borohydride decreases;

2) During hydrogen desorption of $Mg(BH_4)_2$–$NiCl_2$ at 258 ºC and $Mg(BH_4)_2$–NiF_2 at 264 ºC the used additives react with the intermediate boranes to form new compounds with amorphous Ni_3B-like structure;

3) Hydrogen desorption results in the formation of a reversible phase which was identified by ^{11}B NMR as $Mg(B_3H_8)_2$. However, IR could not confirm the presence of the B–H–B bridged bonds, characteristic of $Mg(B_3H_8)_2$;

4) Upon rehydrogenation at pressures between 100 and 150 bar, crystalline β-$Mg(BH_4)_2$ is formed at the expenses of the reversible phase. During hydrogenation, all of the Ni additives, react to form the thermodynamically stable Ni_3B.

These results, compared with previous studies,[10] suggest that the incorporation of Ni additives into $Mg(BH_4)_2$ enhances the kinetics of hydrogen desorption from $Mg(BH_4)_2$. At the same time, interplay of low desorption temperatures and Ni additives possibly limits the formation of higher boranes, which are believed to hinder the reversibility of $Mg(BH_4)_2$. Additional characterization techniques, e.g. ^{11}B solid-state NMR, coupled with advanced modeling methods are required to unambiguously identify the reversible phase found in this work.

5. Acknowledgements

The help from Dr. C. M. Frommen, Dr. J. E. Olsen (preparation of Ni_3B starting material), and Mr. J. Martens (production of the XAFS sample holder) at IFE is gratefully acknowledged. Dr. S. Carlson and Dr. K. Sigfridsson are thanked for assistance and guidance at beamline I811 in Max-Lab, Sweden. This work was supported by the Norwegian Research Council within the NANOMAT (project 182040/S10) and FRIENERGI programs (project 197756/F20), and by the European Fuel Cells and Hydrogen Joint Undertaking (http://www.fch-ju.eu) under collaborative project “BOR4STORE” (Grant agreement no.: N° 303428).

Supporting Information Available

Structural changes observed during the reversible hydrogenation of $Mg(BH_4)_2$ with Ni-based additives

I. Saldan[1,2], S. Hino[1], T. D. Humphries[1], O. Zavorotynska[1], M. Chong[3], C.M. Jensen[3], S. Deledda[1], B.C. Hauback[1]*

[1]Institute for Energy Technology, Physics Department, P.O. Box 40, NO-2027 Kjeller, Norway, Tel:+47 6380-6078 Fax:+47 6381-0920, e-mail: bjorn.hauback@ife.no

[2]Ivan Franko National University of L'viv, Department of Physical and Colloid Chemistry, 6 Kyryla and Mefodia Str., UA-79005 L'viv, Ukraine

[3]University of Hawaii, Department of Chemistry, Honolulu, HI 96822, USA

*Corresponding author

This information is available free of charge via the Internet at http://pubs.acs.org

References

(1) Orimo, S.; Nakamori, Y.; Eliseo, J. R.; Züttel, A.; Jensen, C. M. Complex Hydrides for Hydrogen Storage. *Chem. Rev.* **2007**, *107*, 4111–4132.

(2) Riktor, M. D.; Sørby, M. H.; Fichtner, M.; Chłopek, K.; Buchter, F.; Züttel, A.; Hauback, B. C. *In Situ* Synchrotron Diffraction Studies of Phase Transitions and Thermal Decomposition of $Mg(BH_4)_2$ and $Ca(BH_4)_2$. *J. Mater. Chem.* **2007**, *17*, 4939–4942.

(3) Chłopek, K.; Frommen, C.; Leon, A.; Zabara, O.; Fichtner M. Synthesis and Properties of Magnesium Tetrahydroborate, $Mg(BH_4)_2$. *J. Mater. Chem.* **2007**, *17*, 1396–3503.

(4) Li, H. W.; Kikuchi, K.; Nakamori, Y.; Ohba, N.; Miwa, K.; Towata, S.; Orimo S. Dehydriding and Rehydriding Processes of Well-Crystallized $Mg(BH_4)_2$ accompanying with formation of intermediate compounds. *Acta Mater.* **2008**, *56*, 1342–1347.

(5) Soloveychik, G.; Gao, Y.; Rijssenbeek, J.; Andrus, M.; Kniajanski, S.; Bowman, R. C.; Hwang, S. J.; Zhao Ch. Magnesium Borohydride as a Hydrogen Storage Material: Properties and Dehydrogenation Pathway of Unsolvated $Mg(BH_4)_2$. *J. Hydrogen Energy* **2009**, *34*, 916–928.

(6) Rönnebro E. Development of Group II Borohydrides as Hydrogen Storage Materials. *Cur. Opi. Sol. St. Mater. Sci.* **2011**, *15*, 44–51.

(7) Ozoliņš, V.; Majzoub, E. H.; Wolverton, C. First-Principles Prediction of Thermodynamically Reversible Hydrogen Storage Reactions in the Li-Mg-Ca-B-H system. *J. Am. Chem. Soc.* **2009**, *131*, 230–237.

(8) Hwang, S.; Bowman, R. C.; Reiter, J. J. W.; Rijssenbeek, J.; Soloveichik, G. L.; Zhao, J.; Kabbour, H.; Ahn, C. C. NMR Confirmation for Formation of $[B_{12}H_{12}]^{2-}$ Complexes

during Hydrogen Desorption from Metal Borohydrides. *J. Phys. Chem. C* **2008**, *112*, 3164–3169.

(9) Li, H. W.; Miwa, K.; Ohba, N.; Fujita, T.; Sato, T.; Yan, Y.; Towata, S.; Chen, M.W.; Orimo, S. Formation of an Intermediate Compound with a $B_{12}H_{12}$ Cluster: Experimental and Theoretical Studies on Magnesium Borohydride $Mg(BH_4)_2$. *Nanotecnology* **2009**, *20*, 204013.

(10) Chong, M.; Karkamkar, A.; Autrey, T.; Orimo, S.; Jalisatgi, S.; Jensen, C.M. Reversible Dehydrogenation of Magnesium Borohydride to Magnesium Triborane in the Solid State under Moderate Conditions. *Chem. Comm.* **2011**, *47*, 1330–1332.

(11) Barkhordarian, G.; Klassen, T.; Borman, R. Catalytic Mechanism of Transition-Metal Compounds on Mg Hydrogen Sorption Reaction. *J. Phys. Chem. B* **2006**, *110*, 11020–11024.

(12) Ignatov, A. Yu.; Graetz, J.; Chaudhuri, S.; Salguero, T. T.; Vajo, J. J.; Meyer, F. E. Pinkerton, M.S.; Tyson, T. A. Spatial Configurations of Ti- and Ni- Species Catalyzing Complex Metal Hydrides: X-Ray Absorption Studies and First-Principles DFT and MD Calculations. *AIP Conf. Proc.* **2007**, *882*, 642–644.

(13) Graetz, J.; Chaudhuri, S.; Salguero, T. T.; Vajo, J J; Meyer, M. S.; Pinkerton, F. E. Local Bonding and Atomic Environments in Ni-catalyzed Complex Hydrides. *Nanotechnology* **2009**, *20*, 204007–204015.

(14) Jiang, Z.; Yang, H.; Wei, Z.; Xie, Z.; Zhong, W.; Wie, S. Catalytic Properties and Structures of Nano-Amorphous Ni–B Alloys Affected by Annealing Temperatures. *Appl. Cat. A: Gen.* **2005**, *279*, 165–171.

(15) Humphries, T. D.; Kalantzopoulos, G. N.; Llamas-Jansa, I.; Olsen, J. E.; Hauback, B. C. Reversible Hydrogenation Studies of $NaBH_4$ Milled with Ni-Containing Additives. *J. Phys. Chem. C* **2013**, *117*, 6060–6065.

(16) Kapfenberger, C.; Hofmann, K.; Albert. B. Room-Temperature Synthesis of Metal Borides. *Sol. St. Sci.* **2003**, *5*, 925–930.

(17) Brinks, H. W.; Fossdal, A.; Bowman R. C.; Hauback, B. C. Pressure–composition isotherms of $TbNiAlH_x$. *J. Alloys Comp.* **2006**, *417*, 92–95.

(18) Carlson, S.; Clausen, M.; Gridneva, L.; Sommarin, B.; Svensson, C. XAFS Experiments at Beamline I811, MAX-Lab Synchrotron Source, Sweden. *J. Synchrotron Rad.* **2006**, *13*, 359–364.

(19) Ravel B., Newville M. ATHENA, ARTEMIS, HEPHAESTUS: Data Analysis for X-Ray Absorption Spectroscopy Using IFEFFIT. *J. Synchrotron Rad.* **2005**, ***12***, 537–541.

(20) Aftandilian, V. D.; Miller, H. C.; Muetterties, E. L.; Parshall, G. W. Chemistry of Boranes. V. First Example of a B_{11} Hydride, the $B_{11}H_{14}$- Anion. *Inorg. Chem.* **1962**, *1*, 734–737.

(21) Muetterties, E. L.; Balthis, J. H.; Miller, H. C.; Chia, Y. T.; Knoth, W. H. Chemistry of Boranes. VIII. Salts and Acids of $B_{10}H_{10}^{-2}$ and $B_{12}H_{12}^{-2}$. *Inorg. Chem.* 1964, *3*, 444–451.

(22) Tiritiris, I.; Schleid, T. Die Dodekahydro-*closo*-Dodekaborate $M_2[B_{12}H_{12}]$ der Schweren Alkalimetalle (M^+=K^+,Rb^+,NH_4^+,Cs^+) und Ihre Formalen Iodid-Addukte $M_3I[B_{12}H_{12}]$ (≡MI · $M_2[B_{12}H_{12}]$). *Z. Anorg. Allg. Chem.* **2003**, *629*, 1390–1402.

(23) Li, H. W.; Kikuchi, K.; Nakamori, Y.; Miwa, K.; Towata, S.; Orimo, S. Effects of Ball Milling and Additives on Dehydriding Behaviors of Well-Crystallized $Mg(BH_4)_2$. *Scripta Mater.* **2007**, *57*, 679–682.

(24) Filinchuk, Y.; Richter, B.; Jensen, T. R.; Dmitriev, V.; Chernyshov, D.; Hagemann, H. Porous and Dense $Mg(BH_4)_2$ Frameworks: Synthesis, Stability and Reversible Absorption of Guest Species. *Angew. Chem.* **2011,** *50*, 11162–11166.

(25) Paskevicius, M.; Pitt, M. P.; Webb, C. J.; Sheppard, D. A.; Filsø, U.; Gray, E. M.; Buckley, C. E. In-Situ X-ray Diffraction Study of γ-$Mg(BH_4)_2$ Decomposition. *J. Phys. Chem.C* **2012**, *116*, 15231−15240.

(26) Wei, S.; Oyanagi, H.; Li, Z.; Zhang, X.; Liu, W.; Yin, S.; Wang, X. X-ray-Absorption Fine Structure Study on Devitrification of Ultrafine Amorphous Ni-B Alloys. *Phys. Rev. B* **2001**, *63*, 224201–224206.

(27) Wei, Z.; Li, Z.; Jiang, Z.; Ye, J.; Zhong, W.; Song, J.; Wei, S. In-Situ XAFS Study on Structures and Devitrifications of Ni–B Nano-Amorphous Alloys. *J. Alloys and Comp.* **2008**, *460*, 553–558.

(28) Wei, S.; Li, Z.; Yin, S.; Zhang, X.; Liu, W.; Wang, X. Annealed Crystallization of Ultrafine Amorphous NiB Alloy Studied by XAFS. *J. Synchrotron Rad.* **2001**, *8*, 566–568.

(29) Wei, Z.; Jiang, Z.; Ye, J.; Zhong, W.; Song, J.; Wie, S. In-Situ XAFS Investigation of the Crystallization Mechanism of Ni-B Nano-Amorphous Alloy. *AIP Conf. Proc*. **2007**, *882*, 771–773.

(30) Kapfenberger, C. *Synthese und Charakterisierung von nano-skaligen Nickelboriden*; PhD thesis. Hamburg University Press: Hamburg, Germany. **2005**.

(31) Choi Y.J., Lu J., Sohn H.Y., Fang Z.Z., Kim C., Bowman R.C. , Jr., Hwang S.J. Reaction Mechanisms in the Li_3AlH_6/$LiBH_4$ and Al/$LiBH_4$ Systems for Reversible Hydrogen Storage. Part 2: Solid-State NMR Studies. *J. Phys. Chem. C* **2011**, *115*, 6048–6056.

(32) Wrackmeyer B. Indirect Nuclear Spin-Spin Coupling Constants $^{n}J(^{11}B, ^{1}H)$ and $^{n}J(^{11}B, ^{11}B)$ in Some Boron Hydrides - Density Functional Theory (DFT) Calculation. *Z. Naturforsch.* **2004,** *59b*, 1192–1199.

(33) Giannasi, A.; Colognesi, D.; Ulivi, L.; Zoppi, M.; Ramirez-Cuesta, A. J.; Bardaji, E. G.; Roehm, E.; Fichtner, M. High Resolution Raman and Neutron Investigation of $Mg(BH_4)_2$ in an Extensive Temperature Range. *J. Phys. Chem. A* **2010,** *114*, 2788–2793.

(34) Leites, L. A. Vibrational Spectroscopy of Carboranes and Parent Boranes and its Capabilities in Carborane Chemistry. *Chem. Rev.* **1992,** *92*, 279–323.

Figure and table captions

Table 1. Experimental conditions and hydrogen storage capacities during desorption and hydrogen re-absorption for $Mg(BH_4)_2$–Ni_{add} (Ni_{add} = Ni; $NiCl_2$; NiF_2; Ni_3B) composites.

Fig. 1. PXD patterns for $Mg(BH_4)_2$–Ni_{add}, Ni_{add} = (*a*) Ni_{nano}; (*b*) $NiCl_2$; (*c*) NiF_2; (*d*) Ni_3B, composites (i) as milled; (ii) after hydrogen desorption, and (iii) after hydrogen absorption. Additional impurity of Cu_2O detected for $Mg(BH_4)_2$–Ni_{nano} composites in Fig. 1*a* after absorption is due to contamination during preparation of the PXD specimen.

Fig. 2. Normalized X-ray absorption spectra of $Mg(BH_4)_2$–Ni_{add}, Ni_{add} = Ni_{nano}; $NiCl_2$; NiF_2; Ni_3B, composites (*a*) after milling and *(b)* after hydrogen desorption-absorption.

Fig. 3. Fourier Transform of k^3-weighted $\chi(k)$ function of (*a*) $Mg(BH_4)_2$–Ni_{nano}, (*b*) $Mg(BH_4)_2$–$NiCl_2$, (*c*) $Mg(BH_4)_2$–NiF_2 and (*d*) $Mg(BH_4)_2$–Ni_3B composites in the as-milled state (mil), after the 1st hydrogen desorption (des) and following absorption (abs) together with corresponding Ni additive as reference (ref).

Fig. 4. Fourier Transform of k^3-weighted $\chi(k)$ function of $Mg(BH_4)_2$–Ni_{add}, Ni_{add} = Ni_{nano}; $NiCl_2$; NiF_2; Ni_3B, composites after hydrogen desorption-absorption; synthesized Ni_3B as reference and calculated crystalline Ni_3B.

Fig. 5. Stacked ^1H NMR spectra of $Mg(BH_4)_2$–Ni_{add} composites after desorption and absorption. All samples measures in D_2O solvent.

Fig. 6. Stacked decoupled ^{11}B NMR spectra of $Mg(BH_4)_2$–Ni_{add} composites after desorption and absorption. All samples measures in D_2O solvent.

Table 2. Integrated relative concentrations of polyboranes in $Mg(BH_4)_2$–Ni_{add}, Ni_{add} = Ni_{nano}; $NiCl_2$; NiF_2; Ni_3B, composites in D_2O solution after hydrogen desorption-absorption and pure γ-$Mg(BH_4)_2$ detected by ^{11}B NMR spectroscopy. Chemical shifts: $[BH_4]^-$ –42 ppm; $[B_2H_6]^{2-}$ – 21 ppm; $[B_3H_8]^-$ –31 ppm; $[B_5H_8]^-$ –13 ppm; $[B_{10}H_{10}]^{2-}$ –30 ppm; $[B_{12}H_{12}]^{2-}$ –15 ppm.

Fig. 7. The IR of $Mg(BH_4)_2$–Ni_{add}, Ni_{add} = Ni_{nano}; $NiCl_2$; NiF_2; Ni_3B, composites and starting **γ**-$Mg(BH_4)_2$. The peaks present in **γ**-$Mg(BH_4)_2$ are indicated with dashed lines. The spectra are offset in the vertical direction for better representation and comparison.

Table 1

General parameters of hydrogen desorption-absorption	$Mg(BH_4)_2$–Ni_{add} composite			
	Ni_{nano}	$NiCl_2$	NiF_2	Ni_3B
Desorption temperature (ºC)	256	258	264	220
Absorption temperature (ºC)	251	253	262	210
Absorption pressure (bar)	140	140	100	155
H_2 desorbed (wt. %)	2.7	2.7	6.5	2.7
H_2 absorbed (wt. %)	1.3	1.2	2.0	1.0

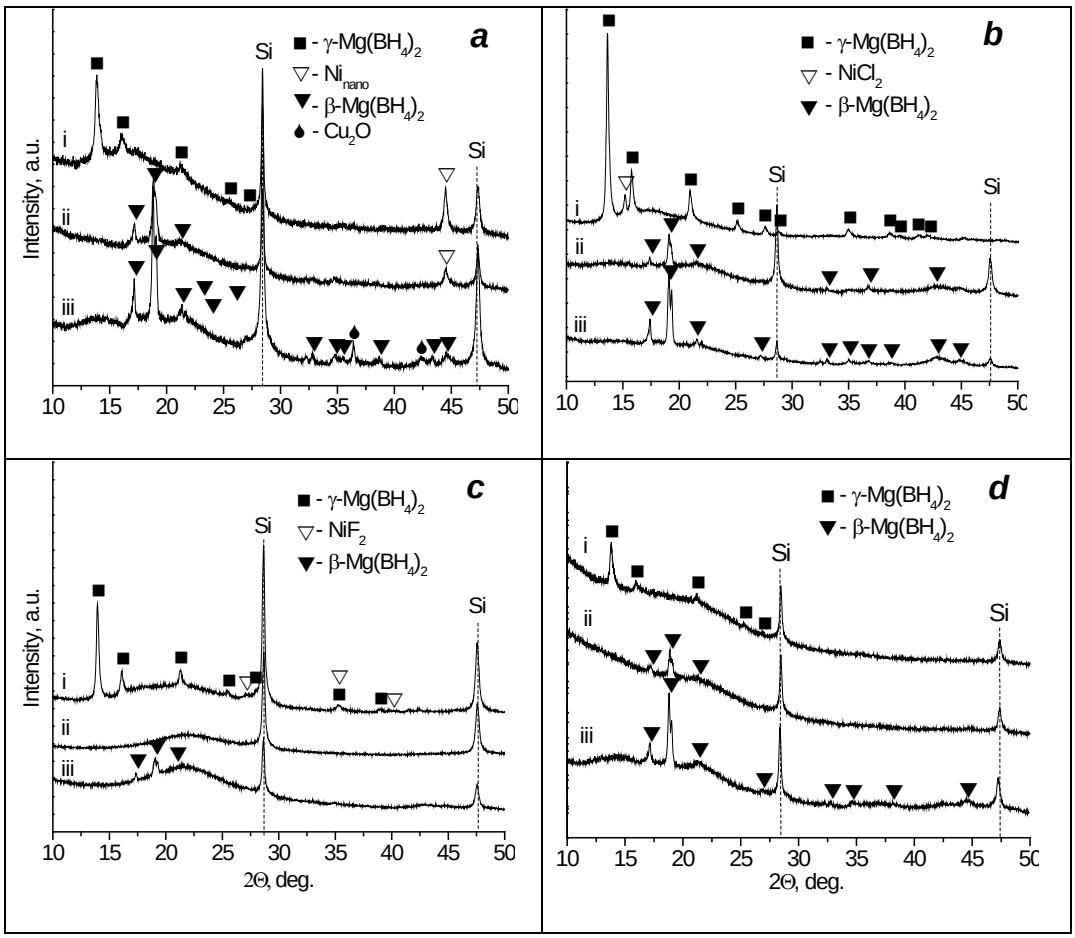
a
■ - γ-Mg(BH4)2
▽- Ninano
▼- β-Mg(BH4)2
♦ - Cu2O
Si
Si
i
ii
iii
Intensity, a.u.
10 15 20 25 30 35 40 45 50
b
■ - γ-Mg(BH4)2
▽ - NiCl2
▼ - β-Mg(BH4)2
Si
Si
i
ii
iii
10 15 20 25 30 35 40 45 50
c
■ - γ-Mg(BH4)2
▽- NiF2
▼- β-Mg(BH4)2
Si
Si
i
ii
iii
Intensity, a.u.
10 15 20 25 30 35 40 45 50
2Θ, deg.
d
■ - γ-Mg(BH4)2
▼ - β-Mg(BH4)2
Si
Si
i
ii
iii
10 15 20 25 30 35 40 45 50
2Θ, deg.

Fig.1

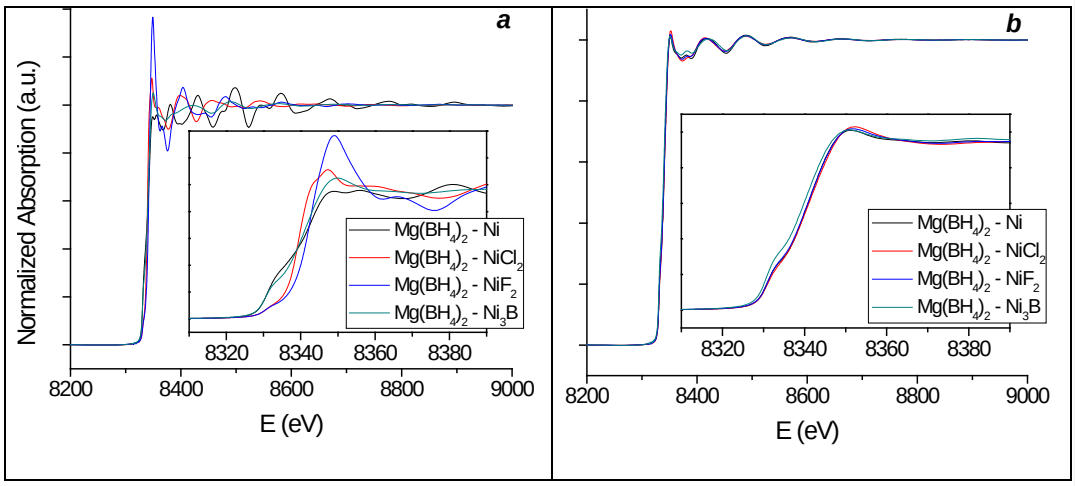
a
b
Normalized Absorption (a.u.)
E (eV)
8200
8400
8600
8800
9000
8320
8340
8360
8380
Mg(BH4)2 - Ni
Mg(BH4)2 - NiCl2
Mg(BH4)2 - NiF2
Mg(BH4)2 - Ni3B

Fig. 2

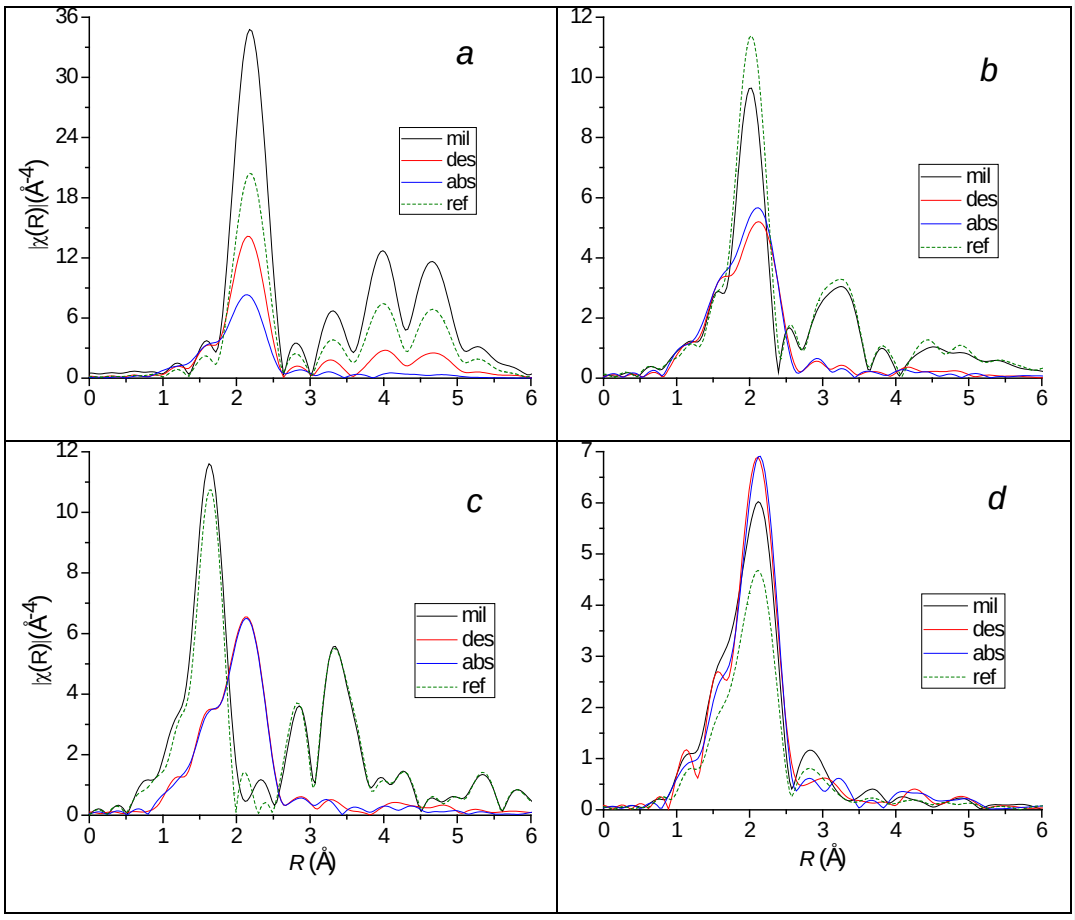

Fig. 3

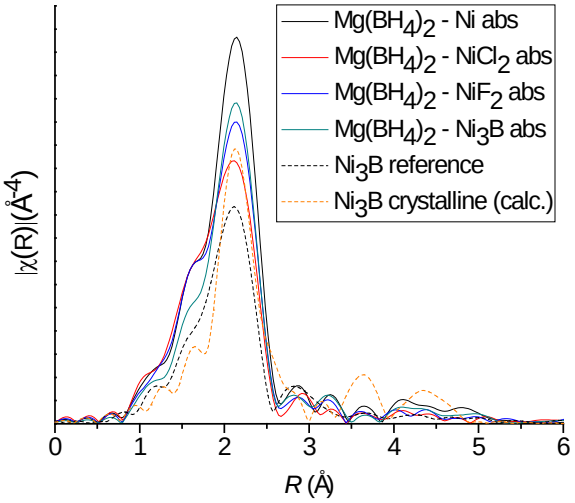
Mg(BH4)2 - Ni abs
Mg(BH4)2 - NiCl2 abs
Mg(BH4)2 - NiF2 abs
Mg(BH4)2 - Ni3B abs
Ni3B reference
Ni3B crystalline (calc.)
|χ(R)|(Å-4)
0
1
2
3
4
5
6
R (Å)

Fig. 4

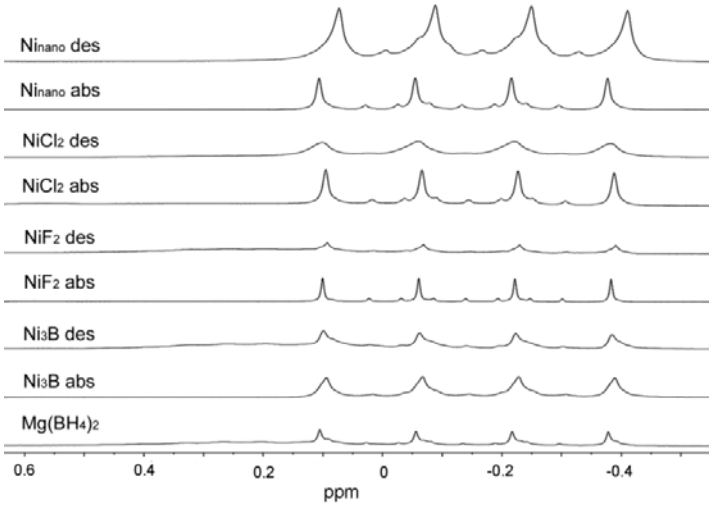
Ninano des
Ninano abs
NiCl2 des
NiCl2 abs
NiF2 des
NiF2 abs
Ni3B des
Ni3B abs
Mg(BH4)2
0.6
0.4
0.2
0
-0.2
-0.4
ppm

Fig. 5

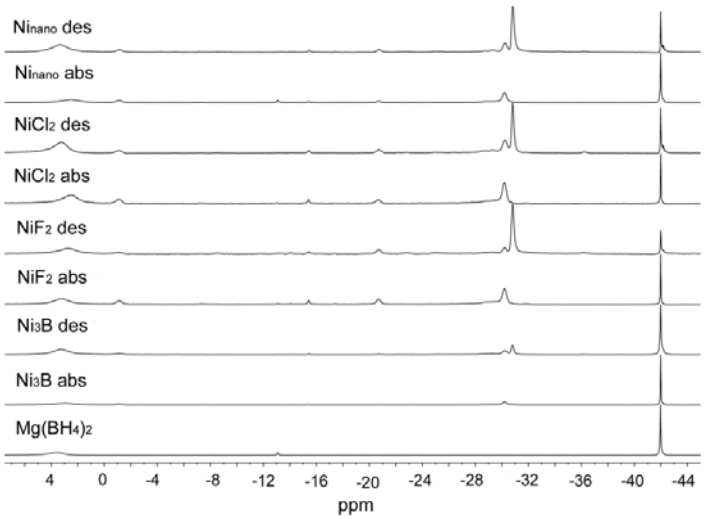
Ninano des
Ninano abs
NiCl2 des
NiCl2 abs
NiF2 des
NiF2 abs
Ni3B des
Ni3B abs
Mg(BH4)2
4
0
-4
-8
-12
-16
-20
-24
-28
-32
-36
-40
-44
ppm

Fig. 6

Table 2

Sample	Borane Species					
	$[BH_4]^-$	$[B_2H_6]^{2-}$	$[B_3H_8]^-$	$[B_5H_8]^-$	$[B_{10}H_{10}]^{2-}$	$[B_{12}H_{12}]^{2-}$
Ni_{nano} des	0.25	0.09	1.00	0.00	0.35	0.03
Ni_{nano} abs	0.94	0.11	0.00	0.09	1.00	0.04
$NiCl_2$ des	0.31	0.13	1.00	0.00	0.47	0.05
$NiCl_2$ abs	0.26	0.14	0.00	0.00	1.00	0.07
NiF_2 des	0.18	0.13	1.00	0.02	0.15	0.03
NiF_2 abs	0.34	0.27	0.06	0.01	1.00	0.08
Ni_3B des	1.00	0.01	0.38	0.00	0.23	0.01
Ni_3B abs	1.00	0.01	0.04	0.00	0.40	0.01
γ-$Mg(BH_4)_2$	1.00	0.00	0.00	0.08	0.00	0.00

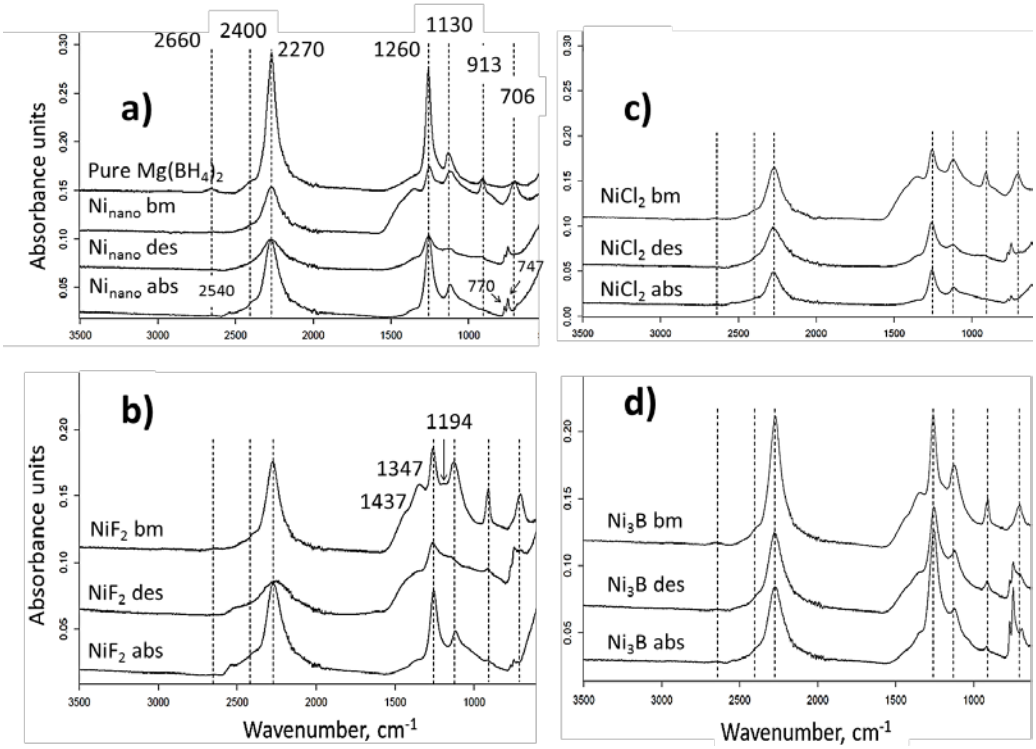
a)
2660
2400
2270
1260
1130
913
706
Pure Mg(BH4)2
Ninano bm
Ninano des
Ninano abs
2540
770
747
Absorbance units
c)
NiCl2 bm
NiCl2 des
NiCl2 abs
b)
1194
1347
1437
NiF2 bm
NiF2 des
NiF2 abs
Wavenumber, cm-1
d)
Ni3B bm
Ni3B des
Ni3B abs
Wavenumber, cm-1

Fig. 7

Graphical abstract

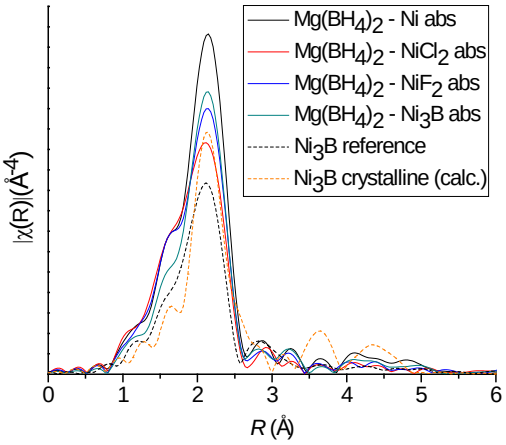

Fourier Transform of k^3-weighted $\chi(k)$ function of $Mg(BH_4)_2$–Ni_{add}, Ni_{add} = Ni_{nano}; $NiCl_2$; NiF_2; Ni_3B, composites after hydrogen desorption-absorption; synthesized Ni_3B as reference and calculated crystalline Ni_3B.

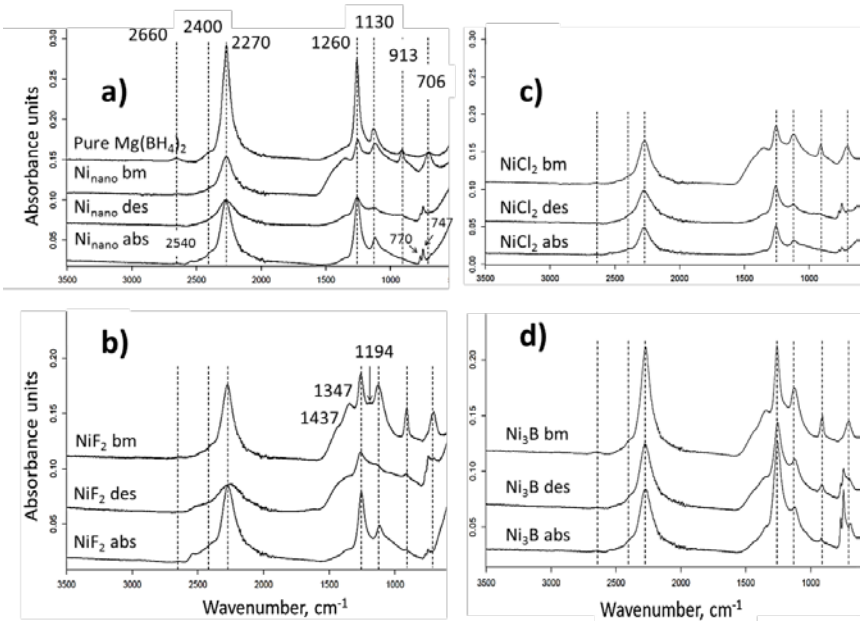

The IR of $Mg(BH_4)_2$–Ni_{add}, Ni_{add} = Ni_{nano}; $NiCl_2$; NiF_2; Ni_3B, composites and starting **γ**-$Mg(BH_4)_2$. The peaks present in **γ**-$Mg(BH_4)_2$ are indicated with dashed lines. The spectra are offset in the vertical direction for better representation and comparison.